Magnetic characterization of λ-MnO_2 and $Li_2Mn_2O_4$ prepared by electrochemical cycling of $LiMn_2O_4$

Young-Il Jang, Biying Huang, F. C. Chou, Donald R. Sadoway, and Yet-Ming Chiang[a)]
Department of Materials Science and Engineering and Center for Materials Science and Engineering, Massachusetts Institute of Technology, Cambridge, Massachusetts 02139

(Received 3 August 1999; accepted for publication 15 February 2000)

Magnetic characterization has been performed on the cubic phases λ-$Li_{0.07}Mn_2O_4$, $Li_{0.98}Mn_2O_4$, and the tetragonal phase $Li_{1.82}Mn_2O_4$, prepared by electrochemical cycling of a single starting $LiMn_2O_4$ spinel. The magnitude of the negative Weiss constant increases with x in $Li_xMn_2O_4$, indicating that antiferromagnetic interactions increase in strength as the Mn^{4+} concentration decreases. Spin-glass behavior is observed in all three materials, as previously seen in nearly stoichiometric $LiMn_2O_4$ [Jang *et al.*, Appl. Phys. Lett. **74**, 2504 (1999)]. A short-range antiferromagnetic correlation is observed in $Li_2Mn_2O_4$ at temperatures below the paramagnetic temperature regime, which is ascribed to collective Jahn–Teller distortion causing a two-dimensional nearest-Mn-neighbors interaction. © *2000 American Institute of Physics.* [S0021-8979(00)05910-7]

INTRODUCTION

$LiMn_2O_4$ spinel (space group $Fd\bar{3}m$) is of interest as a low-cost, high energy density intercalation cathode material for rechargeable lithium batteries.[1,2] The Li and Mn ions are located on the 8*a* tetrahedral sites and the 16*d* octahedral sites, respectively, in the nearly cubic-close-packed oxygen sublattice (32*e* sites). Neighboring MnO_6 octahedra share a common edge. Extraction of Li from $LiMn_2O_4$ leads to formation of λ-MnO_2 (space group $Fd\bar{3}m$),[3,4] while insertion of Li toward the $Li_2Mn_2O_4$ composition gives rise to collective Jahn–Teller (JT) distortion resulting in a tetragonal symmetry (space group $I4_1/amd$) due to the high-spin Mn^{3+} ($t_{2g}^3e_g^1$).[4] $Li_xMn_2O_4$ spinel has interesting magnetic properties as well. From the viewpoint of magnetic interactions, both direct ($Mn^{3+/4+}$–$Mn^{3+/4+}$) and superexchange (90° $Mn^{3+/4+}$–O^{2-}–$Mn^{3+/4+}$) interactions are conceivable between the nearest Mn neighbors. According to Goodenough,[5] only Mn^{4+}–O^{2-}–Mn^{4+} is in ferromagnetic coupling, while all other interactions are in antiferromagnetic coupling. The $[Mn_2]O_4$ spinel framework is retained while the average Mn valence changes upon Li insertion/extraction.[2] The magnetic properties are determined by interactions between the Mn ions, which in turn depend on the Mn valence distribution in the $[Mn_2]O_4$ framework.[6]

In the paramagnetic temperature regime, antiferromagnetic interactions predominate in $Li_xMn_2O_4$ ($x=0,1,2$).[6–16] In λ-MnO_2 and $LiMn_2O_4$, Greedan *et al.*[14] and Wills *et al.*[15] have obtained evidence for long-range antiferromagnetic ordering, resulting in magnetic unit cells containing 128 and 1152 spins below 32 and 65 K, respectively.[14,15] At the other concentration limit, $Li_2Mn_2O_4$, Wills *et al.*[16] reported two-dimensional short-range antiferromagnetic correlation, but no long-range ordering. The complexity of the magnetic structure has been attributed to geometrical frustration inherent in the Mn sublattice.[14–16] Figure 1 shows the structure of $[Mn_2]O_4$ spinel framework and the frustrated antiferromagnetic interaction between the nearest neighbor Mn ions forming the tetrahedron *ABCD*. Recently, we reported the observation of spin-glass behavior in $LiMn_2O_4$ at temperatures below the paramagnetic regime, indicating the presence of frozen spins below a freezing temperature T_f.[1] The existence of frozen spins is consistent with the previous report that a significant fraction of spins remains disordered well below the Néel temperature.[15] In this case, the disordered spins undergo spin-glass ordering at T_f rather than remaining truly disordered (paramagnetic).[1] Spin freezing was also observed in a neutron diffraction study by Oohara *et al.*[17] Possible explanations for the coexistence of spin-glass behavior and antiferromagnetic ordering were given in Ref. 1.

The possible presence of disordered spins has not been explored in λ-MnO_2 and $Li_2Mn_2O_4$.[14,16] It has been unclear whether these phases also exhibit spin-glass behavior in addition to long- and short-range antiferromagnetic ordering, respectively. In this study, we characterized the magnetic properties of a single starting $Li_xMn_2O_4$ spinel in which the Li content (x) was varied solely by electrochemical extraction and insertion. As a result, the $[Mn_2]O_4$ sublattice remains unchanged except for changes in valence accompanying Li intercalation/deintercalation. Since the Li ions are nonmagnetic (diamagnetic), their effect on the magnetic properties is essentially through the Mn valence. This allows an ideal study of the effect of Mn valence on the magnetic properties of a fixed $[Mn]_2O_4$ spinel framework. We show that both the nearly fully delithiated and lithiated end members, λ-MnO_2 and $Li_2Mn_2O_4$, do exhibit spin-glass behavior. A possible effect of the JT distortion on the short-range antiferromagnetic interaction is discussed.

a)Author to whom correspondence should be addressed; electronic mail: YCHIANG@MIT.EDU

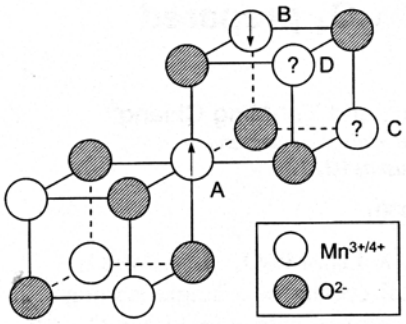

FIG. 1. Structure of $[Mn_2]O_4$ spinel framework. Arrows indicate the direction of the magnetic moment for Mn ions.

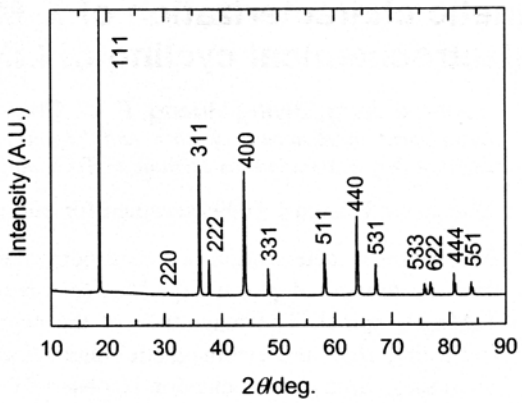

FIG. 2. Powder x-ray diffraction pattern of $LiMn_2O_4$ spinel after firing at 900 °C in air for 4 h. Miller indices hkl are indexed according to the $Fd\bar{3}m$ space group.

EXPERIMENT

Phase-pure $LiMn_2O_4$ spinel was synthesized by firing finely divided, freeze-dried LiOH and Mn_3O_4 precursors at 900 °C in air for 4 h.[1] Details of the sample synthesis are reported elsewhere.[18,19] The oxide powders were characterized by x-ray diffraction (XRD) using Cu $K\alpha$ radiation at 60 kV, 300 mA (Rigaku RTP500RC). Delithiated and lithiated samples were prepared electrochemically using rechargeable Li cells. Cathodes were prepared by mixing together the spinel powder, carbon black (Cabot), graphite (TIMCAL America), and poly(vinylidene fluoride) in the weight ratio of 81:13:1:5. λ-MnO_2 samples were prepared by charging the $LiMn_2O_4$ cathodes to 4.4 V. $Li_2Mn_2O_4$ samples were produced by first charging to 4.4 V, followed by discharging to 2.0 V. A cycled spinel of $\sim LiMn_2O_4$ composition was also produced by charging to 4.4 V and discharging to 3.0 V. Details of Li cell construction are given elsewhere.[20] After the electrochemical treatments, the cells were disassembled in a glove box. Part of each cathode was separated for XRD analysis. Magnetic measurements were carried out on the remaining cathode materials, using a Quantum Design superconducting quantum interference device magnetometer (He atmosphere). The specific magnetization was calculated based on the weight of the oxide alone, after correction for the diamagnetic contribution from the nonoxide components.

RESULTS AND DISCUSSION

Figure 2 shows the powder XRD pattern of the starting $LiMn_2O_4$ after firing at 900 °C in air for 4 h. Note that no impurity phase is detected. Magnetic measurements are sensitive to the presence of impurity phases, including ferrimagnetic Mn_3O_4. The saturation magnetization was determined to be 7.5×10^{-2} and 7.5×10^{-4} emu/g at 30 and 300 K, respectively, from the magnetization curves. A comparison of the magnetization at 30 K (below the Curie temperature for Mn_3O_4 of ~42 K) with literature data[21] indicated a Mn_3O_4 content less than 0.2 wt %. The hkl indices labeled in Fig. 2 are based on the space group $Fd\bar{3}m$. Note that the (220) peak is barely detectable at $2\theta=30.7°$, indicating that most Mn ions are located on the 16d sites, since the (220) peak intensity corresponds to the scattering power of atoms on the 8a sites.[22–24] The lattice parameter for the starting spinel was calculated from the XRD data by a least-squares method to be $a=8.233$ Å, which corresponds to a slightly Li-excess composition ($y\sim0.05-0.09$ in $Li_{1+y}Mn_{2-y}O_4$) according to Ref. 25. The Mn valence is determined by both the Li/Mn and (Li+Mn)/O ratios, which in turn depend on the starting raw materials, firing temperature, and cooling rate.[25,26] The composition of the starting spinel will be indicated by its nominal composition, $LiMn_2O_4$, throughout this paper.

Electrochemical treatments shown in Fig. 3 were used to prepare the phases λ-MnO_2, $LiMn_2O_4$, and $Li_2Mn_2O_4$, for magnetic characterization. The λ-MnO_2 sample was obtained by charging to 4.4 V [Fig. 3(a)], while $LiMn_2O_4$ and $Li_2Mn_2O_4$ samples were obtained by charging to 4.4 V and discharging to 3.0 and 2.0 V, respectively [Figs. 3(b) and 3(c)]. Table I shows for each phase the charge/discharge capacity and the final composition computed on the assumption that the charge/discharge capacity results from Li extraction/insertion only. As can be seen, the compositions approach the fully lithiated and delithiated limits. Hereafter, the samples will be referred to by their compositions in Table I.

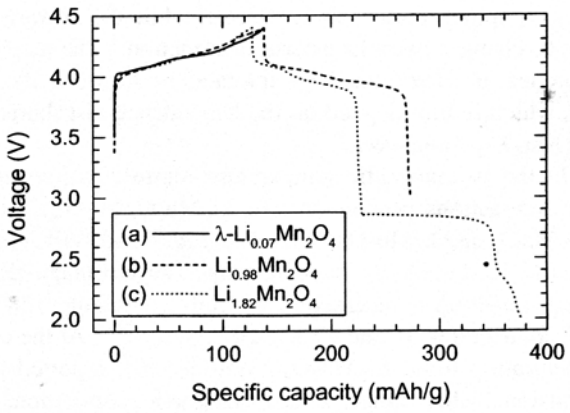

FIG. 3. (a) Electrochemical preparation of λ-$Li_{0.07}Mn_2O_4$ for magnetic characterization. $LiMn_2O_4$ was charged to 4.4 V against a Li metal anode at 8.2 mA/g rate. (b) Electrochemical preparation of $Li_{0.98}Mn_2O_4$ for magnetic characterization. $LiMn_2O_4$ was charged to 4.4 V and discharged to 3.0 V against a Li metal anode at 8.0 mA/g rate. (c) Electrochemical preparation of $Li_{1.82}Mn_2O_4$ for magnetic characterization. $LiMn_2O_4$ was charged to 4.4 V and discharged to 2.0 V against a Li metal anode at 9.7 mA/g rate.

TABLE I. Specific capacity, current density, composition, lattice parameter, Weiss constant, and freezing temperature of λ-$Li_{0.07}Mn_2O_4$, $Li_{0.98}Mn_2O_4$, and $Li_{1.82}Mn_2O_4$ samples prepared by electrochemical cycling of $LiMn_2O_4$.

	Capacity (mAh/g)						
	1st charge (−4.4 V)	1st discharge (3.0–4.4 V)	1st discharge (2.0–3.0 V)	Specific current density (mA/g)	Lattice parameter (Å) (space group)	Weiss constant (K)	Freezing temperature (K)
λ-$Li_{0.07}Mn_2O_4$	137.6	—	—	8.2	$a=8.058$ ($Fd\bar{3}m$)	−74	16
$Li_{0.98}Mn_2O_4$	137.9	134.5	—	8.0	$a=8.230$ ($Fd\bar{3}m$)	−250	25
$Li_{1.82}Mn_2O_4$	127.0	100.7	147.6	9.7	$a=5.654$ $c=9.202$ ($I4_1/amd$)	−770	70

Figure 4 shows the XRD patterns of the composite electrodes, from which the lattice parameters of the oxide phase have been calculated (Table I). The λ-$Li_{0.07}Mn_2O_4$ and $Li_{0.98}Mn_2O_4$ samples are cubic, while the $Li_{1.82}Mn_2O_4$ sample is tetragonal as expected.[2] Note that the $Li_{1.82}Mn_2O_4$ phase clearly shows (400) and (323) peaks at $2\theta=66.1°$ and 67.0°, respectively, with the former being of higher intensity. As shown by diffraction simulations for the tetragonal phase,[27] this allows us to distinguish the tetragonal spinel from the monoclinic phase $LiMnO_2$ of a similar diffraction pattern.

The dc magnetization of the λ-$Li_{0.07}Mn_2O_4$ sample was measured between 5 and 400 K in a magnetic field of 1000 Oe after zero-field cooling (ZFC) and field cooling (FC), respectively [Fig. 5(a)]. The inverse susceptibility is plotted in Fig. 6(a), including a Curie–Weiss law fit to the data above 300 K. The extracted Weiss and Curie constants are $\Theta=-(74\pm5)$ K and $C=(3.23\pm0.03)$ emu K/mol, respectively. A negative Weiss constant indicates that antiferromagnetic Mn^{4+}–Mn^{4+} direct interactions are dominant over ferromagnetic 90° Mn^{4+}–O^{2-}–Mn^{4+} superexchange interactions in the paramagnetic temperature regime.[13] From the Curie constant, the effective moment is determined to be $\mu_{eff}=(3.60\pm0.02)\ \mu_B$ (μ_B being the Bohr magneton, 0.927×10^{-20} erg/Oe), which is smaller than the theoretical spin-only value of 3.87 μ_B for Mn^{4+}. Previously, Goodenough *et al.*[13] reported $\Theta\approx-70$ K,[6] and $\mu_{eff}=3.83\ \mu_B$ for λ-MnO_2 prepared by electrochemical Li extraction from $LiMn_2O_4$, while Greedan *et al.*[14] reported $\Theta=-(104\pm4)$ K and $C=(1.97\pm0.02)$ emu K/mol [corresponding to $\mu_{eff}=(3.97\pm0.02)\ \mu_B$] for λ-$MnO_2$ prepared by the acid leaching of $LiMn_2O_4$ at pH=1. These differing values of Θ and μ_{eff} are

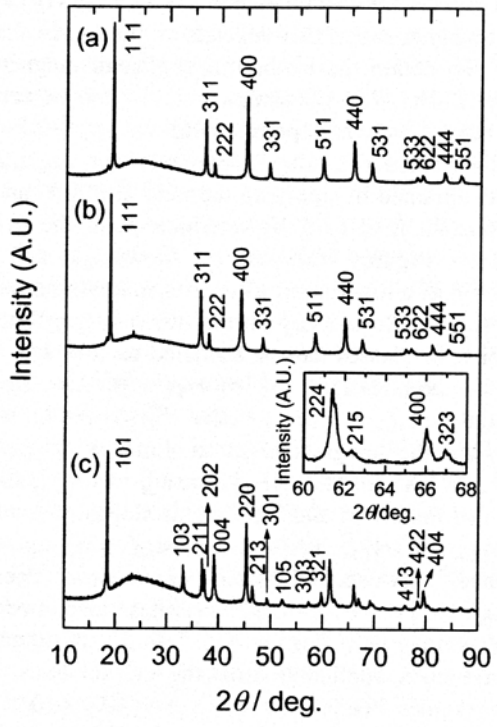

FIG. 4. X-ray diffraction pattern of: (a) λ-$Li_{0.07}Mn_2O_4$, (b) $Li_{0.98}Mn_2O_4$, and (c) $Li_{1.82}Mn_2O_4$ electrodes after electrochemical cycling of $LiMn_2O_4$. Miller indices *hkl* are indexed according to the $Fd\bar{3}m$ space group for (a) and (b), $I4_1/amd$ space group for (c). The inset in (c) identifies the $Li_2Mn_2O_4$ phase as tetragonal.

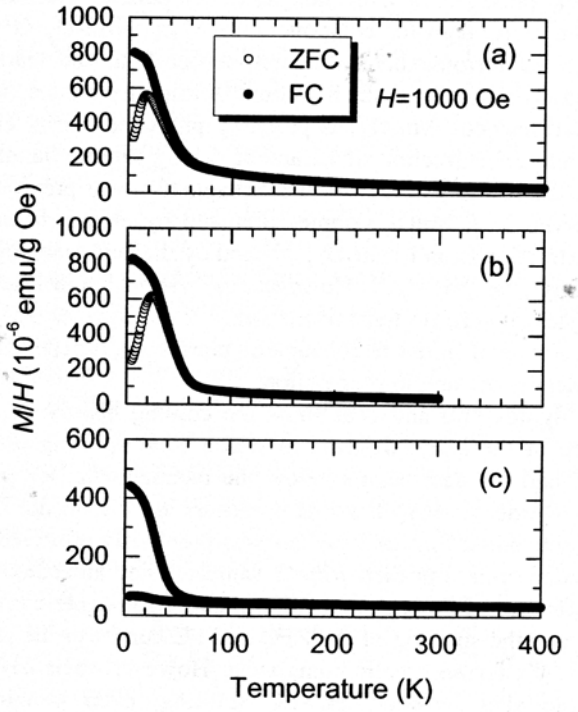

FIG. 5. Zero-field-cooled and field-cooled dc magnetization of: (a) λ-$Li_{0.07}Mn_2O_4$, (b) $Li_{0.98}Mn_2O_4$, and (c) $Li_{1.82}Mn_2O_4$ as a function of temperature in a field of 1000 Oe.

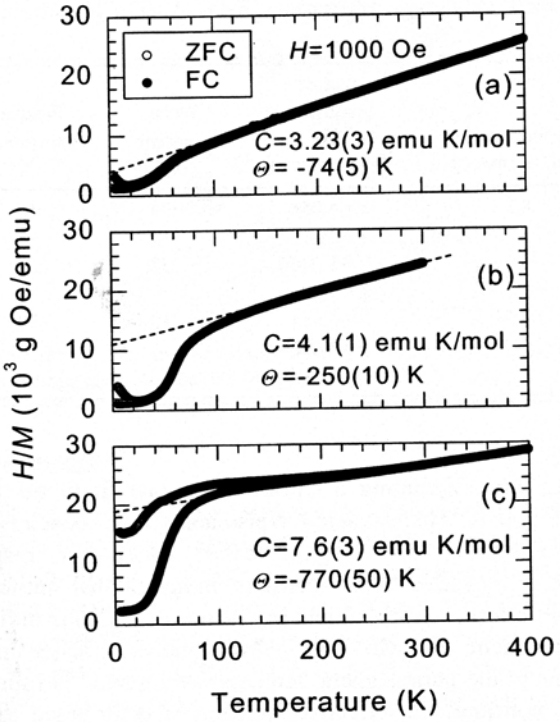

FIG. 6. Inverse zero-field-cooled and field-cooled dc magnetization of λ-$Li_{0.07}Mn_2O_4$, (b) $Li_{0.98}Mn_2O_4$, and (c) $Li_{1.82}Mn_2O_4$ as a function of temperature in a field of 1000 Oe.

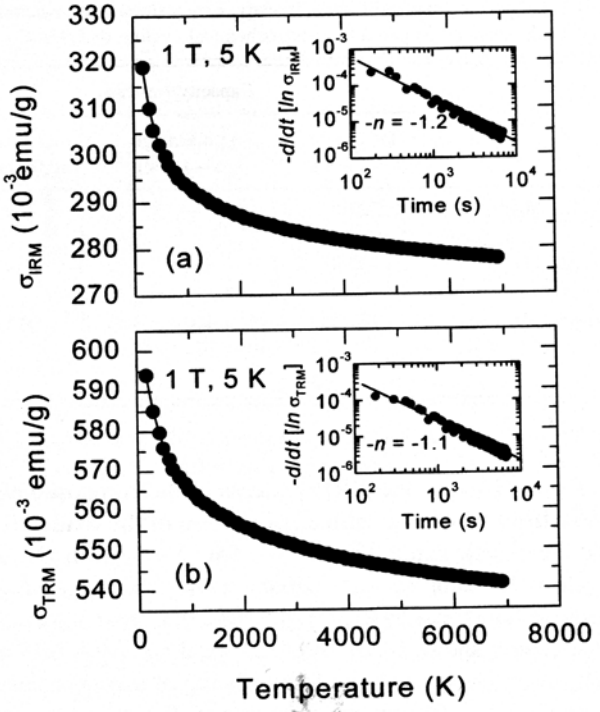

FIG. 7. Time dependence of: (a) σ_{IRM} and (b) σ_{TRM} of λ-$Li_{0.07}Mn_2O_4$ at 5 K after a field of 1 T is set to zero.

possibly due to slight differences in the composition or homogeneity of the samples, which are likely to be dependent on the sample preparation method.

In Fig. 5(a), an abrupt increase of magnetization is noticeable with decreasing temperature below ~60 K, indicating the presence of a ferromagnetic component. The origin of the ferromagnetic component in λ-$Li_{0.07}Mn_2O_4$ is not clear. As ferromagnetism is not observed in the starting $LiMn_2O_4$ samples,[1] a small amount of impurity phases, such as ferrimagnetic Mn_3O_4, is probably produced during electrochemical extraction of Li and/or during sample handling after disassembly of the cell. Ferromagnetism was previously observed in λ-MnO_2 samples prepared by electrochemical Li extraction from $LiMn_2O_4$,[13,14] and by the acid leaching of $LiMn_2O_4$ at pH=2.[14] However, at pH=1, acid-leached samples showed no ferromagnetism.[14] This suggests that the appearance of minor ferromagnetic phases again depends on the details of sample preparation.

Figures 5(a) and 6(b) show the cooling history dependence of the magnetization, in which clear splitting of the ZFC and FC data occurs below the paramagnetic temperature regime. A sharp maximum appears at 16 K in the ZFC magnetization. Similar behavior was previously observed by Greedan *et al.*[14] in their pH=2 sample. They attributed the maximum in ZFC magnetization to antiferromagnetic ordering, and the splitting of the ZFC and FC curves to the presence of a ferromagnetic component. However, their pH=1 sample also showed ZFC–FC splitting, even though it showed no ferromagnetism,[14] indicating that the splitting of the ZFC and FC data is not solely due to the presence of ferromagnetism. Irreversibility in the ZFC and FC magnetization and a maximum in ZFC magnetization at T_f are characteristics of spin glasses.[28] Therefore, we reasoned that the splitting of the ZFC and FC data in Figs. 5(a) and 6(b) is due to spin-glass behavior, even though the presence of ferromagnetism exaggerates the extent of the splitting.

Spin glasses are also characterized by a slowly decaying remanent magnetization that depends on the thermomagnetic history.[28] To obtain the isothermal remanent magnetization σ_{IRM}, the λ-$Li_{0.07}Mn_2O_4$ sample was cooled in zero field from 300 to 5 K, at which point a field was applied for 5 min and then switched off. The thermoremanent magnetization σ_{TRM} was obtained by applying the field at 300 K and cooling in constant field to 5 K, at which point the field was switched off. Figures 7(a) and 7(b) show σ_{IRM} and σ_{TRM}, respectively, as a function of time after removing a field of 1 T. Both show a slow decay on the macroscopic time scale, which for spin glasses can be modeled as a power law ($\sigma = \sigma_0 t^{-a}$), exponential ($\sigma = \sigma_0 \exp[-t]$), or stretched-exponential type ($\sigma = \sigma_0 \exp[-(t/\tau)^{1-n}]$) ($0<n<1$), where σ and σ_0 are the magnetization at time $t=0$ and $t>0$, respectively.[28] A plot of $\log\{-d/dt[\ln \sigma]\}$ vs $\log\{t\}$, shown in the insets of Figs. 7(a) and 7(b), yields slopes of $n=1.2$ and 1.1 for σ_{IRM} and σ_{TRM}, respectively, suggesting a power law dependence.[29] A second order exponential decay ($\sigma = \sigma_1 \exp[-t/\tau_1] + \sigma_2 \exp[-t/\tau_2] + \sigma_3$) has also been suggested by Reimer *et al.* for $LiNiO_2$.[30] In Figs. 7(a) and 7(b), this fit has been applied to give the curved lines, plotted for the values $(\sigma_1, \sigma_2, \sigma_3, \tau_1, \tau_2) = (40.9\times10^{-3}$ emu/g, 24.2×10^{-3} emu/g, 276×10^{-3} emu/g, 250 s, 2590 s) and (41.0×10^{-3} emu/g, 33.9×10^{-3} emu/g, 538×10^{-3} emu/g, 330 s, 3220 s), respectively.

Regardless of the fitting model, the values of σ_{IRM} and σ_{TRM} are different and nonzero, showing that the remanent

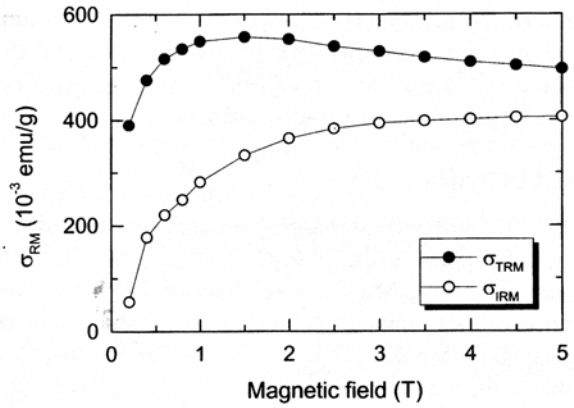

FIG. 8. Field dependence of σ_{IRM} and σ_{TRM} of λ-$Li_{0.07}Mn_2O_4$ at 5 K. Magnetization was measured 1 h after setting the field to zero.

magnetization does depend on the thermomagnetic history, as is typical of spin glasses. The magnetic field dependence of σ_{IRM} and σ_{TRM} at 5 K is shown in Fig. 8 for data obtained at $t=1$ h after the field was switched off. For each condition, the time decay of the magnetization is similar to that shown in Fig. 7. Figure 8 shows that σ_{IRM} increases with increasing field and becomes saturated above 3 T, while σ_{TRM} reaches a maximum at 1.5 T and decreases with increasing field. The difference between σ_{IRM} and σ_{TRM} decreases with increasing field, as is observed in most spin-glass materials.[28]

From these results, it can be concluded that this λ-$Li_{0.07}Mn_2O_4$ material exhibits characteristics of spin-glass behavior in addition to long-range antiferromagnetic ordering.[14] Two possible explanations suggested for the coexistence of spin-glass behavior and antiferromagnetic ordering in $LiMn_2O_4$ (Ref. 1) may be applied to λ-MnO_2 as well. First, the fundamental freezing entities may be antiferromagnetic clusters with finite correlation length and not individual spins, forming a cluster spin glass below the freezing temperature.[31] Second, spatial segregation of antiferromagnetic regions with either infinite or finite correlation length and spin-glass ordered regions may explain the coexistence of antiferromagnetism and spin-glass behavior. Such a complex magnetic structure can be attributed to the inherent geometrical frustration of the antiferromagnetic tetrahedral networks and magnetic disorder arising from a small fraction of randomly distributed residual Li^+ ions causing a distribution of Mn^{3+} in the Mn^{4+} matrix.

It is interesting to compare the magnetic properties of the once-cycled $LiMn_2O_4$ to previous results on the same, but uncycled spinel.[1] Figure 5(b) shows the dc susceptibility of the $Li_{0.98}Mn_2O_4$ sample after the first cycle between 3.0 and 4.4 V [Fig. 3(b)], measured in a magnetic field of 1000 Oe between 5 and 300 K. Ferromagnetism is still observed, indicating the presence of magnetic impurities. Splitting of the ZFC and FC data is again clearly seen, and a sharp maximum appears at 25 K in the ZFC susceptibility, similar to the as-fired $LiMn_2O_4$ samples.[1] Compared to λ-$Li_{0.07}Mn_2O_4$, the higher T_f of ~25 K is consistent with the observation by Endres *et al.*[9] that T_f increases with decreasing Mn valence. For the present sample, a Curie constant $C=(4.1\pm0.1)$ emu K/mol [corresponding to $\mu_{eff}=(4.05\pm0.05)\,\mu_B$], and Weiss constant $\Theta=-(250\pm10)$ K were determined from the linear region in the inverse susceptibility in Fig. 6(b). These results suggest that spins freeze at higher temperatures as the strength of the antiferromagnetic interaction increases. An empirical measure of frustration in spin glasses is the ratio $f=|\Theta|/T_f$.[32] From literature data[1,6–15] and this study, a higher value of f is calculated for $LiMn_2O_4$ ($f=10-14$) than for λ-MnO_2 ($f=5-6$).

The tetragonal spinel sample $Li_{1.82}Mn_2O_4$ also showed the characteristics of spin-glass behavior. Figure 5(c) shows the dc susceptibility after the first cycle between 2.0 and 4.4 V [Fig. 3(c)], measured in a magnetic field of 1000 Oe between 5 and 400 K. The sharp increase in FC susceptibility with decreasing temperature below ~60 K is again seen, indicating the presence of magnetic impurities. From the inverse susceptibility [Fig. 6(c)], the Curie constant is $C=(7.6\pm0.3)$ emu K/mol [corresponding to $\mu_{eff}=(5.5\pm0.1)\,\mu_B$], and the Weiss constant is $\Theta=-(770\pm50)$ K. The latter is more negative compared to λ-$Li_{0.07}Mn_2O_4$ and $Li_{0.98}Mn_2O_4$, as expected from the reduced ferromagnetic Mn^{4+}–O^{2-}–Mn^{4+} coupling. The effective moment is larger than the theoretical spin-only value of $4.90\,\mu_B$ for Mn^{3+}, which is attributed to the presence of some Mn^{2+} ($t_{2g}^3e_g^2$) with $\mu_{eff}=5.92\,\mu_B$. Notice in Fig. 3(c) that a voltage plateau appears during discharge below 2.5 V, indicating that a Li-rich phase is formed.[2,33] Even though the overall composition is $x<2$, a minor amount of overlithiated phase may form due to nonuniform Li insertion within the cathode.[24,34,35]

The tetragonal $Li_{1.82}Mn_2O_4$ sample showed an upward deviation from the Curie–Weiss law in the inverse susceptibility at temperatures below the paramagnetic temperature regime [Fig. 6(c)], which was not present in the other two samples [Figs. 6(a) and 6(b)]. This is attributed to a short-range antiferromagnetic spin correlation in the tetragonal phase. Similar behavior is seen in Wills *et al.*'s[16] ZFC data for $Li_2Mn_2O_4$ prepared by the lithiation of $LiMn_2O_4$ using ^{n}Bu–Li. Diffuse neutron diffraction peaks in the form of a Warren function were observed, indicating the presence of two-dimensional short-range antiferromagnetic correlations.[16] Two-dimensional spin correlation was ascribed to the Kagomé lattice corresponding to the (111) plane of the pyrochlore lattice in $[Mn_2]O_4$. However, it is not clear why $Li_2Mn_2O_4$ alone shows the two-dimensional correlation, since the $[Mn_2]O_4$ spinel framework can be deconstructed into Kagomé layers stacked parallel to the body diagonal in λ-MnO_2 and $LiMn_2O_4$ as well.

Note that the two-dimensional short-range ordering is observed only in the JT distorted tetragonal phase. We suggest that the short-range spin correlation is due to the JT distortion in the tetragonal phase. Considering the $[Mn_2]O_4$ framework in Fig. 1, the inter-Mn distance is uniform throughout in cubic λ-MnO_2 and $LiMn_2O_4$ (e.g., $AB=AC=AD=BD=BC=CD$). However, JT distorted tetragonal $Li_2Mn_2O_4$ has two sets of inter-Mn distance (e.g., $AC=BD<AB=AD=BC=CD$, $AB/AC=1.08$). If antiferromagnetic correlation between the nearest neighbors (e.g., $B-D$ and $A-C$) is energetically favored over frustration, two-dimensional antiferromagnetic correlation along the $B-D$ and $A-C$ directions is possible at temperatures below

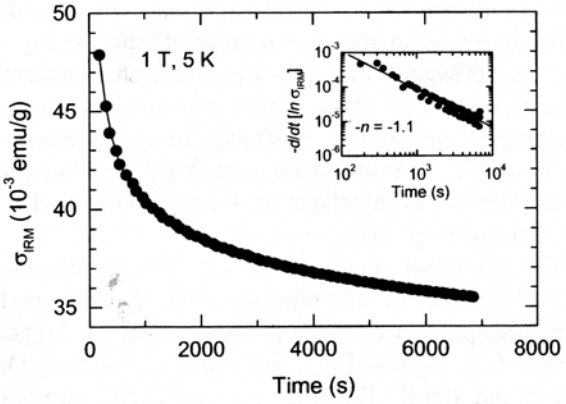

FIG. 9. Time dependence of σ_{IRM} of $Li_{1.82}Mn_2O_4$ at 5 K after a field of 1 T is set to zero.

the paramagnetic temperature regime. Short-range, two-dimensional antiferromagnetic ordering due to the JT distortion has previously been reported for orthorhombic $LiMnO_2$, where the strongest antiferromagnetic exchange interaction is along the direction having the shortest inter-Mn distance.[36]

The time dependence of remanent magnetization is quite similar to that of the other samples (Fig. 9). Fitting results for the stretched-exponential function are shown in the insets, plotted for the values $(\sigma_1,\sigma_2,\sigma_3,\tau_1,\tau_2)=(12.5\times10^{-3}$ emu/g,7.5×10^{-3} emu/g,35.0×10^{-3} emu/g,230 s,2730 s) in Fig. 9, respectively. Since a sharp maximum is not apparent in the ZFC susceptibility in Fig. 5(c), we determined T_f from the temperature below which σ_{IRM} shows relaxation behavior. Figure 10 shows the time decay of σ_{IRM} after a field of 1 T is set to zero at temperatures between 60 and 75 K. The slow decay disappears above 70 K, from which we determine that $T_f=70\pm5$ K in $Li_{1.82}Mn_2O_4$. Clearly this tetragonal spinel phase also exhibits spin-glass behavior in addition to two-dimensional short-range antiferromagnetic ordering.

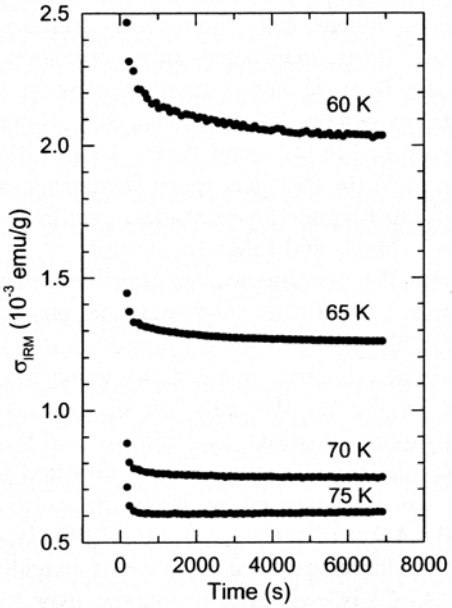

FIG. 10. Time dependence σ_{IRM} of $Li_{1.82}Mn_2O_4$ after a field of 1 T is set to zero at temperatures between 60 and 75 K.

Geometrical frustration remains present, although the antiferromagnetic tetrahedral network is now distorted due to the JT distortion. A distribution of Mn^{3+}, Mn^{4+}, and possibly Mn^{2+} can contribute to magnetic disorder.

CONCLUSIONS

By charging and discharging a single starting $LiMn_2O_4$ spinel, cubic phase λ-$Li_{0.07}Mn_2O_4$ and $Li_{0.98}Mn_2O_4$, and tetragonal phase $Li_{1.82}Mn_2O_4$ were obtained. Magnetic characterization of these samples showed a small contribution from ferromagnetic impurity phases produced by cycling. In the paramagnetic temperature regime, all three phases have a negative Weiss constant, indicating that antiferromagnetic interactions are dominant. The magnitude of the Weiss constant increases with x in $Li_xMn_2O_4$ between the three end members, as the decreasing Mn^{4+} concentration responsible for ferromagnetic Mn^{4+}–O^{2-}–Mn^{4+} interaction decreases. Spin-glass behavior is observed in all three samples. Geometrical frustration due to the antiferromagnetic tetrahedral network in the $[Mn_2]O_4$ spinel structure, combined with some magnetic disorder due to the presence of a valence distribution in the Mn ions, is believed to be responsible for the complex magnetic structure. In $Li_{1.82}Mn_2O_4$, a short-range antiferromagnetic correlation is also observed, possibly due to JT distortion of the tetrahedral network favoring antiferromagnetic correlation between nearest Mn neighbors.

ACKNOWLEDGMENTS

This study was supported by NSF Grant No. 9400334-DMR, and used instrumentation in the Shared Experimental Facilities at MIT. Partial support (for B.H.) was provided by Intronics and the Office of Naval Research (Grant No. 00014-99-1-0565). MIT contributed matching funds from the MacVicar Foundation in the form of a faculty fellowship (for D.R.S.).

[1] Y.-I. Jang, F. C. Chou, and Y.-M. Chiang, Appl. Phys. Lett. **74**, 2504 (1999).
[2] M. M. Thackeray, Prog. Solid State Chem. **25**, 1 (1997).
[3] J. C. Hunter, J. Solid State Chem. **39**, 142 (1981).
[4] A. Mosbah, A. Verbaere, and M. Tournoux, Mater. Res. Bull. **18**, 1375 (1983).
[5] J. B. Goodenough, *Magnetism and the Chemical Bond* (Wiley, New York, 1963).
[6] C. Masquelier, M. Tabuchi, K. Ado, R. Kanno, Y. Kobayashi, Y. Maki, O. Nakamura, and J. B. Goodenough, J. Solid State Chem. **123**, 255 (1996).
[7] G. Blasse, J. Phys. Chem. Solids **27**, 383 (1966).
[8] L. Shütte, G. Cosmann, and B. Reuter, J. Solid State Chem. **27**, 227 (1979).
[9] P. Endres, B. Fuchs, S. Kemmler-Sack, K. Brandt, F. Faust-Becker, and H.-W. Prass, Solid State Ionics **89**, 221 (1996).
[10] N. Kumagai, T. Fujiwara, K. Tanno, and T. Horiba, J. Electrochem. Soc. **143**, 1007 (1996).
[11] Y. Shimakawa, T. Numata, and J. Tabuchi, J. Solid State Chem. **131**, 138 (1997).
[12] J. Sugiyama, T. Hioki, S. Noda, and M. Kontani, Mater. Sci. Eng. B **54**, 73 (1998).
[13] J. B. Goodenough, A. Manthiram, A. C. W. P. James, and P. Strobel, Mater. Res. Soc. Symp. Proc. **135**, 391 (1989).
[14] J. E. Greedan, N. P. Raju, A. S. Wills, C. Morin, S. M. Shaw, and J. N. Reimers, Chem. Mater. **10**, 3058 (1998).
[15] A. S. Wills, N. P. Raju, and J. E. Greedan, Chem. Mater. **11**, 1510 (1999).
[16] A. S. Wills, N. P. Raju, C. Morin, and J. E. Greedan, Chem. Mater. **11**, 1936 (1999).

[17] Y. Oohara, J. Sugiyama, and M. Kontani, J. Phys. Soc. Jpn. **68**, 242 (1999).
[18] Y.-M. Chiang, Y.-I. Jang, H. Wang, B. Huang, D. R. Sadoway, and P. Ye, J. Electrochem. Soc. **145**, 887 (1998).
[19] Y.-I. Jang, H. Wang, and Y.-M. Chiang, J. Mater. Chem. **8**, 2761 (1998).
[20] B. Huang, Y.-I. Jang, Y.-M. Chiang, and D. R. Sadoway, J. Appl. Electrochem. **28**, 1365 (1998).
[21] K. Dwight and N. Menyuk, Phys. Rev. **119**, 1470 (1960).
[22] D. G. Wickham and W. J. Croft, J. Phys. Chem. Solids **7**, 351 (1958).
[23] M. R. Richard, E. W. Fuller, and J. R. Dahn, Solid State Ionics **73**, 81 (1994).
[24] H. Wang, Y.-I. Jang, B. Huang, D. R. Sadoway, and Y.-M. Chiang, J. Electrochem. Soc. **146**, 473 (1999).
[25] Y. Gao and J. R. Dahn, J. Electrochem. Soc. **143**, 100 (1996).
[26] J. M. Tarascon, E. Wang, F. K. Shokoohi, W. R. McKinnon, and S. Colson, J. Electrochem. Soc. **138**, 2859 (1991).
[27] Y.-I. Jang, B. Huang, Y.-M. Chiang, and D. R. Sadoway, Electrochem. Solid-State Lett. **1**, 13 (1998).
[28] K. Binder and A. P. Young, Rev. Mod. Phys. **58**, 802 (1986).
[29] R. V. Chamberlin, J. Appl. Phys. **57**, 3377 (1985).
[30] J. N. Reimers, J. R. Dahn, J. E. Greedan, C. V. Stager, G. Liu, I. Davidson, and U. von Sacken, J. Solid State Chem. **102**, 542 (1993).
[31] J. L. Tholence and R. Tournier, J. Phys. (France) **35**, C4-229 (1974).
[32] A. P. Ramirez, Annu. Rev. Mater. Sci. **24**, 453 (1994).
[33] W. I. F. David, J. B. Goodenough, M. M. Thackeray, and M. G. S. R. Thomas, Rev. Chim. Miner. **20**, 636 (1983).
[34] Y.-I. Jang, B. Huang, H. Wang, D. R. Sadoway, and Y.-M. Chiang, J. Electrochem. Soc. **146**, 3217 (1999).
[35] H. Wang, Y.-I. Jang, and Y.-M. Chiang, Electrochem. Solid-State Lett. **2**, 490 (1999).
[36] J. E. Greedan and N. P. Raju, J. Solid State Chem. **128**, 209 (1997).